


Superresolution capacity of variance-based stochastic fluorescence microscopy: From random illumination microscopy to superresolved optical fluctuation imaging

Simon Labouesse,¹ Jérôme Idier,² Marc Allain,³ Guillaume Giroussens³,³ Thomas Mangeat,¹ and Anne Sentenac^{3,*}

¹*LITC Core Facility, Centre de Biologie Intégrative, Université de Toulouse, CNRS, UPS, 31062 Toulouse, France*

²*Nantes Université, École Centrale Nantes, CNRS, LS2N, 44300 Nantes, France*

³*Aix Marseille Univ, CNRS, Centrale Marseille, Institut Fresnel, 13013 Marseille, France*

 (Received 19 June 2023; revised 10 March 2024; accepted 12 March 2024; published 28 March 2024)

Improving the resolution of fluorescence microscopy beyond the diffraction limit can be achieved by acquiring and processing multiple images of the sample under different illumination patterns (periodic grids, focused beams, or more generally speckles). When the illuminations are known, the superresolved reconstruction is generally formed from a linear combination of the multiple diffraction-limited images, and the resolution gain is easily determined. On the other hand, when the illuminations are unknown, the resolution gain is seldom well defined. In this work, we consider the recent random illumination microscopy (RIM) technique where the illuminations are unknown speckles and the reconstructions are formed from the variance of the images. We show that an unambiguous twofold resolution gain can be obtained only when the speckle correlation length coincides with the width of the observation point spread function. Last, we analyze the difference between the variance-based techniques using random speckled illuminations (as in RIM) and those obtained using random fluorophore activation (as in superresolution optical fluctuation imaging).

DOI: [10.1103/PhysRevA.109.033525](https://doi.org/10.1103/PhysRevA.109.033525)

I. INTRODUCTION

The light intensity recorded by the camera of a fluorescence microscope cannot exhibit spatial frequencies above $2/\lambda$ where λ is the wavelength of the emitted light. This low-pass filtering, due to the loss of the evanescent waves at the detector plane, cannot be circumvented. Therefore the challenge of superresolution imaging is to recover spatial frequencies of the sample fluorescence density beyond $2/\lambda$ from data that are frequency limited to $2/\lambda$. A widespread solution consists in processing multiple images obtained by changing the illumination, such as translating focused spots [1–4] or rotating and translating periodic light patterns [5,6]. The data processing of most techniques using structured illuminations requires the knowledge of the illumination patterns, either explicitly as in structured illumination microscopy [5,6] or implicitly as in confocal or image scanning microscopy [1]. In this context, random illumination microscopy (RIM) [7] stands out as an exception as it does not require knowledge of the illumination patterns: the superresolved image is formed from the variance of multiple diffraction-limited images recorded under different random speckled illuminations. While attractive because of its simplicity and significant image improvement [7], RIM variance-based processing lacks a rigorous analysis of its resolution potential, the nonlinearity of the variance being a significant obstacle to its derivation. In this work, we study the sample information that can be extracted from the variance of speckled images as a function of the statistical properties of the random illumination and we

derive the condition under which the variance can provide a resolution gain.

II. DEFINING THE RESOLUTION IN THE SPATIAL FREQUENCY SPACE

To model the data provided by a fluorescence microscope under an inhomogeneous illumination, we introduce the point spread function of the microscope h and the illumination intensity function E . Importantly, these two functions are defined at a macroscopic scale inside the sample, through the averaging over regions large enough to contain thousands of atoms (typically of the order of a thousand nm^3), to wash out the microscopic fluctuations. In this context, we define the macroscopic fluorescence density ρ such that $V\rho(\mathbf{r})E(\mathbf{r})$ is the energy (detected by the camera) of the fluorescent light emitted by a macroscopic volume V centered about \mathbf{r} . Hereafter we neglect the Poisson noise. The fluorescence density depends on the fluorophore concentration and the molecular brightness.

With these definitions, the microscope image can be written as,

$$I(\mathbf{r}) = \int \rho(\mathbf{r}')E(\mathbf{r}')h(\mathbf{r} - \mathbf{r}')d\mathbf{r}', \quad (1)$$

where \mathbf{r} indicates a position in the image domain that is conjugated to a point in the object domain. This model can be applied to two- or three-dimensional (3D) imaging configurations. In the spatial frequency space (Fourier space), Eq. (1) reads,

$$\tilde{I}(\mathbf{v}) = \tilde{h}(\mathbf{v}) \int \tilde{\rho}(\mathbf{v} - \mathbf{v}')\tilde{E}(\mathbf{v}')d\mathbf{v}', \quad (2)$$

*anne.sentenac@fresnel.fr

where $\tilde{f}(\mathbf{v}) = \int f(\mathbf{r})e^{-i2\pi\mathbf{v}\cdot\mathbf{r}}d\mathbf{r}$ stands for the Fourier transform of f .

If E is a constant, as in a standard fluorescence microscope, the recorded image depends only on the sample spatial frequencies belonging to the support of the optical transfer function (OTF) \tilde{h} , noted W_h , which is at best a disk of radius $2/\lambda$ (in the 2D case) or exhibits a toruslike shape in the 3D case [8].

We now consider cases where the illumination E is inhomogeneous. In periodic structured illumination microscopy (SIM), the illumination is a periodic light grid generally formed from the interference of two or three collimated laser beams that is translated and rotated [6]. In point-scanning microscopy, the illumination is a focused beam that is scanned across the sample [4]. In random illumination microscopy, the illumination is a random speckle obtained, for example, by passing a laser beam through a diffuser. Noting W_E the support of \tilde{E} , the recorded image depends on the sample spatial frequencies in the domain

$$W_{hE} = \{\mathbf{v} - \boldsymbol{\mu} \mid \mathbf{v} \in W_h, \boldsymbol{\mu} \in W_E\}, \quad (3)$$

which is no longer limited by $2/\lambda$ and corresponds to the frequency support of hE .

Yet, sensitivity to spatial frequencies of the sample outside W_h is a necessary but not a sufficient condition for being able to form a superresolved image. One also needs a technique for extracting the high spatial frequencies of the sample from the diffraction-limited images I_n obtained for various illumination intensities E_n . Hereafter, the gain of resolution of a superresolved technique will be measured through the ability to recover $\tilde{\rho}$ beyond W_h .

III. RESOLUTION OF TECHNIQUES USING KNOWN INHOMOGENEOUS ILLUMINATIONS

When the illumination function is well known, as in periodic SIM or point-scanning microscopy, the superresolved image is obtained through a linear combination of the recorded data, and the superresolution capacity of the technique is easily determined. In periodic SIM, the sample is illuminated successively by N different light grids $E_{n=1\dots N}$. The resolution of a system of linear equations permits the recovery of the object spatial frequencies in $\bigcup_{n=1}^N W_{hE_n}$ [6].

In point-scanning microscopy, one records images for different positions of a focused illumination. We note $E(\mathbf{r})$ the illumination intensity at \mathbf{r} when the beam is focused at the origin. The image that is recorded when the illumination is focused at \mathbf{r}_o reads,

$$I(\mathbf{r}, \mathbf{r}_o) = \int \rho(\mathbf{r}')E(\mathbf{r}' - \mathbf{r}_o)h(\mathbf{r} - \mathbf{r}')d\mathbf{r}'. \quad (4)$$

Taking the Fourier transform of $I(\mathbf{r}, \mathbf{r}_o)$ with respect to $(\mathbf{r}, \mathbf{r}_o)$ yields,

$$\tilde{I}(\mathbf{v}, \mathbf{v}_o) = \tilde{h}(\mathbf{v})\tilde{\rho}(\mathbf{v} - \mathbf{v}_o)\tilde{E}(\mathbf{v}_o). \quad (5)$$

In theory, it is possible to recover the sample frequencies $\tilde{\rho}(\boldsymbol{\mu})$ for any $\boldsymbol{\mu} \in W_{hE}$ whatever the shape of the translated illumination. Yet, in practice, this reconstruction scheme is never used. In confocal microscopy, for example, the superresolved image is obtained without numerical processing, by simply

recording the signal at the (conjugated) position of the focused beam, $I_{SR}(\mathbf{r}) = I(\mathbf{r}, \mathbf{r}) = \int \rho(\mathbf{r}')E(\mathbf{r}' - \mathbf{r})h(\mathbf{r} - \mathbf{r}')d\mathbf{r}'$. The frequency support of the function $E(-\mathbf{u})h(\mathbf{u})$ being W_{hE} , the confocal approach directly recovers the sample frequencies over the whole accessible superresolved domain. Yet, this ideal resolution requires the use of an infinitely small pinhole, which is impossible in practice.

We now turn to microscopy configurations where the inhomogeneous illuminations are unknown. These approaches ease the experimental implementation, as the control of the illuminations becomes minimal, but require more complex reconstruction schemes.

IV. RESOLUTION OF TECHNIQUES USING RANDOM ILLUMINATIONS (RIM)

In the last 15 years, it was observed that superresolved images of the sample could be built from multiple low-resolution images acquired with random speckled illuminations. The first reconstruction techniques [9–12] estimated both the sample and the illuminations using advanced regularization techniques, such as sparsity or binarity. The complexity of the reconstruction procedures and the influence of the regularization in the final result prevented any rigorous determination of the superresolution capacity of these approaches.

Recently [13], it was proposed to reconstruct the sample from the second-order statistics of the speckled images. The major interest of this statistical approach (known as RIM for random illumination microscopy) is that it does not require the knowledge (nor the estimation) of the illuminations. It only requires the knowledge of the speckle statistics (namely the mean and autocovariance), which are theoretically well defined and very robust to misalignments or aberrations [14]. More precisely, RIM consists in recording multiple images of a sample under different fully developed speckled illuminations E_n . The speckled patterns can be considered different realizations of a second-order stationary random process E , with constant mean $\langle E \rangle$ (where $\langle \cdot \rangle$ indicates the ensemble average) and autocovariance, $C(\mathbf{r} - \mathbf{r}') = \langle E(\mathbf{r})E(\mathbf{r}') \rangle - \langle E \rangle^2$. The frequency support of C is the same as the frequency support of each speckled illumination and is noted W_E [14,15]. It is demonstrated mathematically in Ref. [13] that, if $W_E = W_h$, the sample frequencies in the enlarged domain W_{h^2} can be recovered from the square root of the covariance matrix of the speckled images defined as,

$$\text{Cov}(\mathbf{r}, \mathbf{r}') = \langle I(\mathbf{r})I(\mathbf{r}') \rangle - \langle I(\mathbf{r}) \rangle \langle I(\mathbf{r}') \rangle. \quad (6)$$

Yet, forming the covariance matrix, let alone its square root, is numerically untractable. In practice, RIM reconstruction method, named algoRIM, processes only the variance $V_\rho(\mathbf{r}) = \text{Cov}(\mathbf{r}, \mathbf{r})$ of the speckled images. The sample is estimated iteratively so as to minimize a distance between the experimental variance image V^{exp} and the simulated variance image for a given ρ , V_ρ [7,16]. The minimization procedure is not a simple task as the variance image is quadratically linked to the sample ρ through [7,17]

$$V_\rho(\mathbf{r}) = \int d\mathbf{r}_1 d\mathbf{r}_2 h(\mathbf{r} - \mathbf{r}_1) \times \rho(\mathbf{r}_1)C(\mathbf{r}_1 - \mathbf{r}_2)\rho(\mathbf{r}_2)h(\mathbf{r} - \mathbf{r}_2). \quad (7)$$

On many calibrated and biological samples, RIM exhibited a resolution twice better than that of a classical fluorescence microscope, which indicated that the sample estimated by algoRIM presented spatial frequencies in the enlarged domain W_{h^2} [7,17]. Now, to be fully confident in RIM results, it is necessary to show that the solution of the variance-matching procedure (which ideally provides the same variance image as the experimental one, $V_\rho = V^{\text{exp}}$) has the same spectrum $\tilde{\rho}$ as the actual sample in a domain about W_{h^2} . The question is: if two samples yield the same variance image, do they have the same spectrum in a domain larger than W_h ? If yes, the size of this domain will define RIM superresolution capacity.

We recall that the variance is formed from the square of raw images that are frequency limited to W_h but depend on the sample spectrum in W_{hE} . The variance is sensitive to the spatial frequencies of the sample in W_{hE} (we show on a specific example in Appendix B that this is indeed the case), but its frequency support is W_{h^2} . In other terms, the number of unknowns (the sample frequencies in W_{hE}) is, in general, different from the number of data (the variance frequencies in W_{h^2}). Thus, it is likely that the answer to the question raised above will be different when W_{hE} is the same as, included in, or bigger than, W_{h^2} .

In the classical RIM configuration, the illumination is performed through the same objective as the observation. If the Stokes shift can be neglected [7,14] the frequency support of the speckled illumination W_E is the same as that of the point spread function, W_h . Hence, the frequency support of the variance W_{h^2} matches the support of the sample spectrum it depends on, W_{hE} . In this case, we demonstrate in Appendix A that if two samples have the same variance image, they have necessarily the same sample spectrum within W_{h^2} . This result ensures the unicity of the variance-matching solution and determines the superresolution capacity of RIM: RIM achieves the same resolution as an ideal confocal microscope in which the focused beam and the point spread function share the same frequency support.

We now consider the case where the speckle correlation length is larger than the width of the point spread function, i.e., $W_E \subset W_h$. In this case, it is always possible to filter the raw images to transform h into C and the variance of the modified images gives access to the sample spatial frequencies in W_{E^2} at least. Yet, this result is not totally satisfactory. Indeed, in this case, the frequency support of the variance W_{h^2} is larger than the frequency support of the sample spectrum it depends on, W_{hE} . In other terms, we have more data than unknowns. It is likely that, with some approximations, the resolution can be improved further (maybe up to W_{hE}), but this remains to be demonstrated.

Last, we study the configurations where the speckle correlation length is smaller than the width of the point spread function, $W_h \subset W_E$. In this case, we have fewer data than unknowns ($W_{h^2} \subset W_{hE}$), and we foresee major difficulties. Indeed, we show in Appendix B, that there is a loss of information in the variance image that prevents the reconstruction of the sample spectrum in W_{hE} and even in W_{h^2} . In particular, two samples with different spectra in W_{h^2} can provide the same variance image. These issues can be reduced with *a priori* information on the sample and regularization techniques, but the resolution gain, if any, will not be universal. The ambiguity

of the variance image when $W_h \subset W_E$ applies in particular to configurations where the speckles are assumed to be spatially uncorrelated. This assumption amounts to considering that the observation point spread function and the fluorescence density vary slowly over the speckle grain size. This is the case when near-field speckles are used together with far-field detection [18] or optical speckles with acoustic detection [19]. In these techniques, hereafter called speckle-SOFI, the expression of the variance simplifies to,

$$V_{\text{speckle-SOFI}}(\mathbf{r}) \approx C_0 \int h^2(\mathbf{r} - \mathbf{r}') \rho^2(\mathbf{r}') d\mathbf{r}'. \quad (8)$$

where $C_0 = \int C(\mathbf{r}) d\mathbf{r}$. We observe that the variance is now linearly linked to the square of the sought parameter (optical absorption or fluorescence density) that is filtered over W_{h^2} . Now, knowing the Fourier transform of ρ^2 in W_{h^2} does not mean that $\tilde{\rho}$ can be retrieved over W_{h^2} (except if ρ is binary). We show in Appendix B that, when the speckled illumination is spatially uncorrelated, it is possible to find samples with different fluorescence density spectra in W_{h^2} that have the same variance image.

V. RESOLUTION OF TECHNIQUES USING RANDOM ACTIVATION OF THE FLUOROPHORES (SOFI)

In this last section, we differentiate fluctuation imaging using quasiuncorrelated speckled illuminations from super-resolution optical fluctuation imaging (SOFI). In SOFI, the intensity fluctuations observed in the recorded images come from the random activation of the fluorophores and not from the illumination (which is kept homogeneous and equal to E_0 during the whole experiment). To account for this phenomenon, one needs to explain further the characteristics of the fluorescence density ρ , which is related to the fluorophore concentration and the molecular brightness. We define the fluorophore concentration g at the macroscopic scale such that $Vg(\mathbf{r})$ is the number of fluorophores contained in a macroscopic volume V centered about \mathbf{r} . Next, we introduce the mean molecular brightness b , which accounts for the fluorophores' quantum yield and for the environment-dependent ability of the incident (emitted) photons to reach the fluorophore (detector). If all the fluorophores are activated in V , the mean brightness b is defined such that $Vg(\mathbf{r})b(\mathbf{r})E_0$ is the energy measured by the camera of the photons emitted from V . In other terms, if all the fluorophores are activated, the fluorescence density is the product of the fluorophore concentration times the mean brightness, $\rho = g \times b$.

In SOFI, only a few fluorophores of V are activated during the image recording and they change at each novel image. Let us assume that they follow a Poisson point process of intensity proportional to the total number of fluorophores in V . Then, the number of activated fluorophores in V observed when recording one image becomes a Poisson variable of parameter $Vg(\mathbf{r})p(\mathbf{r})$ where p is the mean percentage of activation. Under this assumption, we show in Appendix D that the variance of SOFI images reads,

$$V_{\text{SOFI}}(\mathbf{r}) = E_0^2 \int h^2(\mathbf{r} - \mathbf{r}') b^2(\mathbf{r}') g(\mathbf{r}') p(\mathbf{r}') d\mathbf{r}'. \quad (9)$$

While RIM is able to recover the fluorescence density $\rho = g \times b$ over W_{h^2} , SOFI has a similar superresolution capacity, but the latter applies to a distinct density $g \times b^2 \times p = \rho \times b \times p$.

It is worth noting that if the mean brightness b is homogeneous, RIM and SOFI are able to restore the fluorophore concentration g over W_{h^2} , (provided the mean activation percentage p in SOFI is also homogeneous). On the contrary, even if b is homogeneous, fluctuation imaging using quasi-uncorrelated speckled illuminations (speckle-SOFI) can only restore the square of the fluorophore concentration, g^2 , over W_{h^2} . Thus, SOFI and speckle-SOFI yield *a priori* different results and their umbrella denomination as fluctuation imaging can be misleading.

VI. CONCLUSION

There exist three main superresolved microscopy techniques that form superresolved images from the variance of multiple diffraction-limited images. RIM uses speckled illuminations that are correlated over a distance comparable to the width of the observation point spread function, speckle-SOFI uses quasiuncorrelated speckled illuminations, and SOFI takes advantage of the random activation of fluorophores. In this work, we have shown that while these three techniques can offer a doubling of resolution, this is not applied to the same sample parameters. SOFI recovers the fluorophore concentration times the square of the brightness while speckle-SOFI recovers the square of the fluorophore concentration times the square of the brightness. For its part, RIM recovers the fluorescence density, i.e., the fluorophore concentration times the brightness, in the same way as an ideal confocal microscope. Our demonstration provides a solid theoretical ground for the twofold resolution gain, the optical sectioning, and the linearity to fluorescence observed in the last RIM experiments [7,17].

ACKNOWLEDGMENT

This work was supported by a grant from the Agence Nationale de la Recherche for the project 3D-RIM.

APPENDIX A: SUPERRESOLUTION CAPACITY OF RIM WHEN $W_E = W_h$

In this Appendix, we consider the classical RIM configuration where the speckle autocovariance C is similar to the observation point spread function h . Experimentally, this condition is fulfilled in epifluorescence microscopy when the speckled illumination fills the pupil of the collection objective and the Stokes shift is negligible. In this case, we show that if two samples ρ_1 and ρ_2 have the same variance image, they have the same spectrum in W_{h^2} .

1. Demonstration of the bijection between the variance image and the sample spectrum in W_{h^2}

First of all, we recall that the variance is formed from the square of images acquired under random illuminations whose frequency support W_E is equal to W_h . From Eq. (3) we deduce that the variance is only sensitive to the sample

spectrum in $W_{h^2} = W_{h^2}$. Thus, two samples with the same spectrum in W_{h^2} will provide the same variance image. The reciprocal is significantly more difficult to demonstrate due to the quadratic link between the variance and the sample. It requires the introduction of a bilinear symmetric operator $B_{U,V}$ acting on real integral functions (U, V) ,

$$B_{U,V}(\mathbf{r}) = \int d\mathbf{r}_1 d\mathbf{r}_2 h(\mathbf{r} - \mathbf{r}_1) \times U(\mathbf{r}_1)C(\mathbf{r}_1 - \mathbf{r}_2)V(\mathbf{r}_2)h(\mathbf{r} - \mathbf{r}_2) \quad (\text{A1})$$

such that the variance V_ρ is equal to $B_{\rho,\rho}$.

The bilinear operator $B_{U,V}$ can be cast as the product of linear operators acting on U and V . To this aim, we define h_E such that $\tilde{h}_E = \sqrt{\tilde{C}}$ (we recall that \tilde{C} is always positive as C is an autocovariance function), which satisfies

$$\int h_E(\mathbf{r}_1 - \mathbf{x})h_E(\mathbf{r}_2 - \mathbf{x})d\mathbf{x} = C(\mathbf{r}_1 - \mathbf{r}_2). \quad (\text{A2})$$

Introducing h_E in Eq. (A1), we obtain,

$$B_{U,V}(\mathbf{r}) = \int M_U(\mathbf{r}, \mathbf{x})M_V(\mathbf{r}, \mathbf{x})d\mathbf{x} \quad (\text{A3})$$

with

$$M_V(\mathbf{r}, \mathbf{x}) = \int h(\mathbf{r} - \mathbf{r}_1)V(\mathbf{r}_1)h_E(\mathbf{r}_1 - \mathbf{x})d\mathbf{r}_1. \quad (\text{A4})$$

At this point, we note that the Fourier transform of M_V with respect to (\mathbf{r}, \mathbf{x}) ,

$$\tilde{M}_V(\mathbf{v}, \boldsymbol{\mu}) = \tilde{h}(\mathbf{v})\tilde{V}(\boldsymbol{\mu} + \mathbf{v})\tilde{h}_E(\boldsymbol{\mu}), \quad (\text{A5})$$

is bounded, so M_V is an analytic function. In addition, if $h = C$, we demonstrate (at the end of this section) that,

$$\int B_{U,V}(\mathbf{r})V(\mathbf{r})d\mathbf{r} = \int |M_V(\mathbf{r}, \mathbf{x})|^2 U(\mathbf{r})d\mathbf{r}d\mathbf{x}. \quad (\text{A6})$$

We now consider two fluorescence densities, $\rho_1(\mathbf{r}) \geq 0$ and $\rho_2(\mathbf{r}) \geq 0$ that have the same RIM variance, $B_{\rho_1,\rho_1}(\mathbf{r}) = B_{\rho_2,\rho_2}(\mathbf{r})$. Using the bilinearity and symmetry of $B_{U,V}$, we can show that $B_{\rho_1,\rho_1} - B_{\rho_2,\rho_2} = B_{\rho_1+\rho_2,\rho_1-\rho_2} = 0$. This last property implies, in particular, that,

$$\int B_{\rho_1+\rho_2,\rho_1-\rho_2}(\mathbf{r})[\rho_1(\mathbf{r}) - \rho_2(\mathbf{r})]d\mathbf{r} = 0, \quad (\text{A7})$$

which, using Eq. (A6), can be cast as,

$$\int |M_{\rho_1-\rho_2}(\mathbf{r}, \mathbf{x})|^2 [\rho_1(\mathbf{r}) + \rho_2(\mathbf{r})]d\mathbf{r}d\mathbf{x} = 0. \quad (\text{A8})$$

We now assume that $\rho_1 + \rho_2$ stays strictly positive in a nonempty open set Ω . In this case, Eq. (A8) is satisfied if and only if $M_{\rho_1-\rho_2}(\mathbf{r}, \mathbf{x}) = 0$ for $\mathbf{r} \in \Omega$ and for all \mathbf{x} . Since $M_{\rho_1-\rho_2}$ is analytic, $M_{\rho_1-\rho_2}(\mathbf{r}, \mathbf{x}) = 0$ for all \mathbf{x} and for $\mathbf{r} \in \Omega$ implies that $M_{\rho_1-\rho_2}(\mathbf{r}, \mathbf{x}) = 0$ for all \mathbf{x} and all \mathbf{r} , thus $\tilde{M}_{\rho_1-\rho_2}(\mathbf{v}, \boldsymbol{\mu}) = 0$ for all \mathbf{v} and $\boldsymbol{\mu}$. From Eq. (A5), the nullity of $\tilde{M}_{\rho_1-\rho_2}$ is obtained only if $\tilde{\rho}_1(\boldsymbol{\eta}) - \tilde{\rho}_2(\boldsymbol{\eta}) = 0$ for $\boldsymbol{\eta} \in W_{h^2}$. Hence, if ρ_1 and ρ_2 have the same RIM variance, they have the same spatial frequencies in W_{h^2} .

We have thus demonstrated that there is a one-to-one correspondence between the spatial frequencies of the variance

of diffraction-limited speckled images and the spatial frequencies of the sample fluorescence density in the enlarged frequency domain W_{h^2} provided $C = h$.

2. Proof of Eq. (A6)

The demonstration of Eq. (A6) requires that $h = C$. In this case, Eq. (A1) can be rewritten as,

$$B_{U,V}(\mathbf{r}) = \int d\mathbf{r}_1 d\mathbf{r}_2 h(\mathbf{r} - \mathbf{r}_1) \\ \times U(\mathbf{r}_1)h(\mathbf{r} - \mathbf{r}_2)V(\mathbf{r}_2)h(\mathbf{r}_1 - \mathbf{r}_2).$$

Using $h(\mathbf{r} - \mathbf{r}_2) = \int h_E(\mathbf{r} - \mathbf{x})h_E(\mathbf{r}_2 - \mathbf{x})d\mathbf{x}$, one obtains

$$\int B_{U,V}(\mathbf{r})V(\mathbf{r})d\mathbf{r} \\ = \int d\mathbf{r}d\mathbf{r}_1 d\mathbf{r}_2 d\mathbf{x} h(\mathbf{r} - \mathbf{r}_1)V(\mathbf{r}) \\ \times h_E(\mathbf{r} - \mathbf{x})h(\mathbf{r}_1 - \mathbf{r}_2)V(\mathbf{r}_2)h_E(\mathbf{r}_2 - \mathbf{x})U(\mathbf{r}_1).$$

Recalling the expression of M_V in Eq. (A4) and the symmetry of h and h_E , we get

$$\int B_{U,V}(\mathbf{r})V(\mathbf{r})d\mathbf{r} = \int |M_V(\mathbf{r}_1, \mathbf{x})|^2 U(\mathbf{r}_1) d\mathbf{x} d\mathbf{r}_1.$$

APPENDIX B: WHAT HAPPENS WHEN $W_h \subset W_E$?

We now study the configurations where $W_h \subset W_E$, namely the speckle correlation length is smaller than the width of the point spread function. This situation is encountered with near-field speckles or when the illumination pupil is larger than the collection pupil. In this case, we show that even if the variance is sensitive to the sample spectrum in W_{hE} , there is a loss of information that prevents its recovery. In addition, we show that two samples with different spectra in W_{h^2} can provide the same variance image.

To simplify the discussion, we assume that (W_h, W_E) are centered plain disks with frequency cutoffs ν_h and ν_E , respectively, with $\nu_h < \nu_E$. We further assume that the point spread function h is symmetric so that \tilde{h} is a real positive symmetric function, like \tilde{C} . We consider a sample whose spectrum is restricted to the null frequency and a high frequency $\pm\mathbf{k}$, $\rho(\mathbf{r}) = A + B \cos(2\pi\mathbf{k} \cdot \mathbf{r} + \varphi)$ with (A, B) real positive such that ρ is real positive. The variance of the raw images, given by Eq. (7), obtained with such sample reads,

$$V_\rho(\mathbf{r}) = A^2\alpha + B^2\beta(\mathbf{k}) + 2AB\gamma(\mathbf{k}) \cos(2\pi\mathbf{k} \cdot \mathbf{r} + \varphi) \\ + B^2\eta(\mathbf{k}) \cos(4\pi\mathbf{k} \cdot \mathbf{r} + 2\varphi), \quad (\text{B1})$$

with

$$\alpha = \int |\tilde{h}|^2(\mathbf{v})\tilde{C}(\mathbf{v})d\mathbf{v}, \\ \beta(\mathbf{k}) = \int |\tilde{h}|^2(\mathbf{v} + \mathbf{k})\tilde{C}(\mathbf{v})d\mathbf{v}, \\ \gamma(\mathbf{k}) = \int \tilde{h}(\mathbf{k} - \mathbf{v})\tilde{h}(\mathbf{v})\tilde{C}(\mathbf{v})d\mathbf{v}, \\ \eta(\mathbf{k}) = \int \tilde{h}(\mathbf{v})\tilde{h}(2\mathbf{k} - \mathbf{v})\tilde{C}(\mathbf{k} - \mathbf{v})d\mathbf{v}.$$

We observe that as long as $k < \nu_h + \nu_E$, $\beta(\mathbf{k}) \neq 0$ and the variance depends on the high spatial frequency of the sample, B . This result confirms the sensitivity of the variance to sample spatial frequencies in W_{hE} . However, if $2\nu_h < k \leq \nu_h + \nu_E$, $\gamma(\mathbf{k}) = \eta(\mathbf{k}) = 0$ so that $V_\rho(\mathbf{r}) = \alpha A^2 + \beta(\mathbf{k})B^2$. In this case, the variance is sensitive to the amplitudes of the null and high frequencies of the sample, (A, B) , but it has lost the information about the phase of the high frequency, φ . Worse, this example shows that a uniform sample defined by $\rho_1(\mathbf{r}) = (A^2 + \beta(\mathbf{k})B^2)^{\frac{1}{2}}/\alpha$ will have the same variance as the inhomogeneous sample defined by $\rho(\mathbf{r}) = A + B \cos(2\pi\mathbf{k} \cdot \mathbf{r} + \varphi)$. Thus, when $\nu_h < \nu_E$, the identifiability of the sample spatial frequencies from the variance is lost, even for frequencies belonging to W_{h^2} . This assertion is particularly counterintuitive as it shows that decreasing the size of the speckle grains below the width of the observation point spread function is *a priori* detrimental to the sample reconstruction.

APPENDIX C: IMAGING WITH QUASIUNCORRELATED SPECKLES, SPECKLE-SOFI

When the point spread function and fluorescence density vary slowly over the width of the speckle autocovariance function, the variance of the diffraction-limited images is linearly linked to the square of ρ filtered over W_{h^2} . In this section, we provide an example of two positive functions with different spectra in the superresolved domain W_{h^2} , which, when squared, have exactly the same spectra in W_{h^2} .

We consider g the sum of a constant and a one-dimensional cosine along the x axis with a frequency k laying in W_{h^2} but not in W_h , and f the sum of a constant and two cosines with period k and $2k$. Note that $2k$ lays outside W_{h^2} . We adapt the constant and the cosine amplitudes so that f and g are positive and f^2 and g^2 are equal in W_{h^2} . A possible solution is,

$$f(x) = 6 + \sqrt{2} \cos(2\pi kx) + \cos(4\pi kx) \\ g(x) = \frac{\sqrt{101} + 7}{2\sqrt{2}} + \frac{\sqrt{101} - 7}{2} \cos(2\pi kx). \quad (\text{C1})$$

Noting \mathcal{F} the low-pass filter operator that removes all the frequencies outside W_{h^2} , we find,

$$\mathcal{F}[f^2](x) = \mathcal{F}[g^2](x) = 75 + 13\sqrt{2} \cos(2\pi kx).$$

APPENDIX D: MODELING SOFI AT THE MACROSCOPIC SCALE

Generally, SOFI data are modeled with a discrete sum that depends on the fluorophore positions [20]. However, it is clearly impossible to recover the fluorophores positions from SOFI (second-order) image, except if a constraint of sparsity is assumed. It may thus be interesting to relate SOFI images to sample characteristics that are defined at a macroscopic scale, such as the fluorophore concentration.

In structured illumination microscopy, one assumes that all the fluorophores are activated. The fluorescence density ρ is written as the product of the fluorophore concentration g with a mean brightness b . The intensity recorded by the camera is

modeled as,

$$I(\mathbf{r}) = \int h(\mathbf{r} - \mathbf{r}')E(\mathbf{r}')g(\mathbf{r}')b(\mathbf{r}')d\mathbf{r}', \quad (\text{D1})$$

where E is the inhomogeneous illumination intensity and h the microscope point spread function.

In SOFI, the illumination E_0 is homogeneous but the fluorophores oscillate between an activated and nonactivated state. Thus, only a subset of the fluorophores present in the sample contributes to the image intensity at a given time t . The activated fluorophores in the (macroscopic) volume V centered about \mathbf{r} can be seen as points popping up at random and independently of one another. This process is conveniently modeled with a Poisson point process of intensity proportional to the number of fluorophores in V . Under this assumption, the number of activated fluorophores in V at time t , written as $Vq(\mathbf{r}, t)$, where q is the activated fluorophore concentration,

is a Poisson variable of parameter $Vg(\mathbf{r})p(\mathbf{r})$ with p the mean percentage of activation. With this definition, the intensity of the image recorded at t can be written as,

$$I(\mathbf{r}, t) = E_0 \int h(\mathbf{r} - \mathbf{r}')q(\mathbf{r}', t)b(\mathbf{r}')d\mathbf{r}'. \quad (\text{D2})$$

It is thus a filtered Poisson variable whose time variance reads [21],

$$V_{\text{SOFI}}(\mathbf{r}) = E_0^2 \int h^2(\mathbf{r} - \mathbf{r}')b^2(\mathbf{r}')g(\mathbf{r}')p(\mathbf{r}')d\mathbf{r}'.$$

Note that this result recovers the expression given in the original SOFI paper [20] if one expresses the fluorophore concentration distribution as $\sum_{k=1}^K \delta(\mathbf{r} - \mathbf{r}_k)$ where \mathbf{r}_k is the position of the k th fluorophore.

-
- [1] C. Sheppard and C. Cogswell, Three-dimensional image formation in confocal microscopy, *J. Microsc.* **159**, 179 (1990).
- [2] T. A. Klar and S. W. Hell, Subdiffraction resolution in far-field fluorescence microscopy, *Opt. Lett.* **24**, 954 (1999).
- [3] C. J. R. Sheppard, Super-resolution in confocal imaging, *Optik (Stuttgart)* **80**, 53 (1988).
- [4] C. B. Müller and J. Enderlein, Image scanning microscopy, *Phys. Rev. Lett.* **104**, 198101 (2010).
- [5] R. Heintzmann and C. G. Cremer, Laterally modulated excitation microscopy: improvement of resolution by using a diffraction grating, in *Optical Biopsies and Microscopic Techniques III*, Vol. 3568 (SPIE, Bellingham, 1999), pp. 185–196.
- [6] M. G. Gustafsson, Surpassing the lateral resolution limit by a factor of two using structured illumination microscopy, *J. Microsc.* **198**, 82 (2000).
- [7] T. Mangeat, S. Labouesse, M. Allain, A. Negash, E. Martin, A. Guénolé, R. Poincloux, C. Estibal, A. Bouissou, S. Cantaloube, E. Vega, T. Li, C. Rouvière, S. Allart, D. Keller, V. Debarnot, X. B. Wang, G. Michaux, M. Pinot, R. L. Borgne *et al.*, Super-resolved live-cell imaging using random illumination microscopy, *Cell Rep. Meth.* **1**, 100009 (2021).
- [8] A. Sentenac and J. Mertz, Unified description of three-dimensional optical diffraction microscopy: from transmission microscopy to optical coherence tomography: tutorial, *J. Opt. Soc. Am. A* **35**, 748 (2018).
- [9] E. Mudry, K. Belkebir, J. Girard, J. Savatier, E. Le Moal, C. Nicoletti, M. Allain, and A. Sentenac, Structured illumination microscopy using unknown speckle patterns, *Nature Photonics* **6**, 312 (2012).
- [10] J. Min, J. Jang, D. Keum, S.-W. Ryu, C. Choi, K.-H. Jeong, and J. C. Ye, Fluorescent microscopy beyond diffraction limits using speckle illumination and joint support recovery, *Sci. Rep.* **3**, 2075 (2013).
- [11] L.-H. Yeh, L. Tian, and L. Waller, Structured illumination microscopy with unknown patterns and a statistical prior, *Biomed. Opt. Express* **8**, 695 (2017).
- [12] S. Labouesse, A. Negash, J. Idier, S. Bourguignon, T. Mangeat, P. Liu, A. Sentenac, and M. Allain, Joint reconstruction strategy for structured illumination microscopy with unknown illuminations, *IEEE Trans. Image Process.* **26**, 2480 (2017).
- [13] J. Idier, S. Labouesse, M. Allain, P. Liu, S. Bourguignon, and A. Sentenac, On the superresolution capacity of imagers using unknown speckle illuminations, *IEEE Trans. Comput. Imaging* **4**, 87 (2018).
- [14] J. W. Goodman, *Speckle Phenomena in Optics: Theory and Applications* (SPIE, Bellingham, 2020).
- [15] M. B. Priestley, *Spectral Analysis and Time Series: Probability and Mathematical Statistics* (Academic Press, New York, 1981).
- [16] G. Giroussens, S. Labouesse, M. Allain, T. Mangeat, A. Sentenac, and J. Idier, Fast super-resolved reconstructions in fluorescence random illumination microscopy (RIM), Tech. Rep. <https://hal.science/hal-04139086> (2023).
- [17] K. Affannoukoué, S. Labouesse, G. Maire, L. Gallais, J. Savatier, M. Allain, M. Rasedujjaman, L. Legoff, J. Idier, R. Poincloux, F. Pelletier, C. Letierrier, T. Mangeat, and A. Sentenac, Super-resolved total internal reflection fluorescence microscopy using random illuminations, *Optica* **10**, 1009 (2023).
- [18] Y. Choi, M. Kim, C. Park, J. Park, Y. Park, and Y.-H. Cho, Wide-field superresolution optical fluctuation imaging through dynamic near-field speckle illumination, *Nano Lett.* **22**, 2194 (2022).
- [19] T. Chaigne, J. Gateau, M. Allain, O. Katz, S. Gigan, A. Sentenac, and E. Bossy, Super-resolution photoacoustic fluctuation imaging with multiple speckle illumination, *Optica* **3**, 54 (2016).
- [20] T. Dertinger, R. Colyer, G. Iyer, S. Weiss, and J. Enderlein, Fast, background-free, 3D superresolution optical fluctuation imaging (SOFI), *Proc. Natl. Acad. Sci.* **106**, 22287 (2009).
- [21] D. L. Snyder and M. I. Miller, *Random Point Processes in Time and Space* (Springer, New York, 1991).